Collision Risk Assessment Algorithm via Lane-Based Probabilistic Motion Prediction of Surrounding Vehicles

Jaehwan Kim, *Student Member, IEEE*, and Dongsuk Kum, *Member, IEEE*

***Abstract*— In order to ensure reliable autonomous driving, the system must be able to detect future dangers in sufficient time to avoid or mitigate collisions. In this paper, we propose a collision risk assessment algorithm that can quantitatively assess collision risks for a set of local path candidates via the lane-based probabilistic motion prediction of surrounding vehicles. First, we compute target lane probabilities, which represent how likely a driver is to drive or move toward each lane, based on lateral position and lateral velocity in curvilinear coordinates. And then, collision risks are computed by incorporating both model probability distribution of lanes and a time-to-collision between a pair of predicted trajectories. Finally, collision risks are plotted on a trajectory plane that represents each set of the tangential acceleration and the final lateral offset of local path candidates. This collision risk map provides intuitive risk measures, and can also be utilized to determine a control strategy for a collision avoidance maneuver. Validation of the model is conducted by comparing the model probabilities with the maneuver probabilities derived from the next generation simulation database. Furthermore, the effectiveness of the proposed algorithm is verified in two driving scenarios, preceding vehicle braking and cut-in, on a curved highway with multiple vehicles.**

***Index Terms*— Risk assessment, local path candidates, lane-based probabilistic motion prediction, time-to-collision (TTC), collision risk map, NGSIM trajectory database.**

I. Introduction

A. Background and Motivation

THE development of autonomous driving systems has been an active area of research for the last decade. Among others, global automotive companies such as BMW, Volvo, and Mercedes-Benz have already invested considerable efforts in developing autonomous driving technologies [1]. However, the state-of-the-art technologies are still far from a level of performance that can guarantee public safety and the ability to cope with dangers that may arise from complex and uncertain traffic scenarios. Unless the safety and reliability of these systems can be guaranteed, people and societies are unlikely to accept this potentially intrusive technology. In order to ensure safety, a key enabling technology is a reliable risk assessment, which must be able to predict how collision risks will evolve in the future. For instance, as shown in Fig. 1, the risk level may seem quite low if an algorithm predicts that the vehicle on the left side of the ego vehicle stays in its current lane. However, the risk level associated with the left vehicle can be very high if an algorithm predicts that this vehicle will change its lane towards the ego vehicle. In fact, because the future can never be deterministically known a priori, an algorithm needs to consider both scenarios in a probabilistic manner.

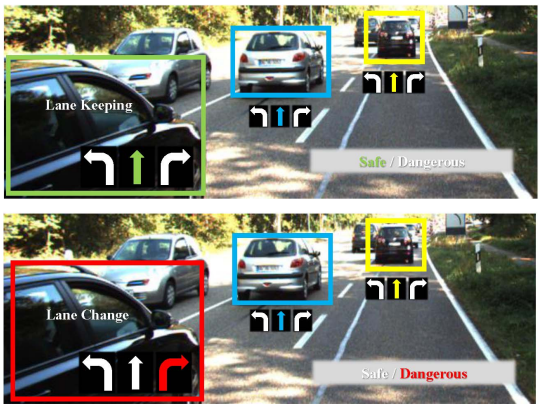

Fig. 1. Two difference future scenarios may be possible for a given situation. Two different motion and risk predictions lead to different control strategies.

B. Literature Review

The existing risk prediction methods can be classified into two categories: deterministic and probabilistic approaches by whether the future motion uncertainty is taken into account or not. Generally, the first approach employs simplified future prediction models such as constant yaw rate and acceleration (CYRA) in order to compute quantitative risk indicator: Time-to-Collision (TTC), Time-to-Brake(TTB), and Time-to-Steer(TTS) [2], [3], [43]. In addition, this approach

Manuscript received September 6, 2016; revised June 6, 2017 and September 13, 2017; accepted October 19, 2017. Date of publication December 6, 2017; date of current version September 7, 2018. This work was supported in part by the Ministry of Science, ICT and Future Planning, Korea, through the Information Technology Research Center Program, supervised by the Institute for Information & Communications Technology Promotion under Grant IITP-2016-R2718-16-0011, and in part by the BK21 Plus Program through the National Research Foundation funded by the Ministry of Education of Korea. The Associate Editor for this paper was S. Sun. *(Corresponding author: Dongsuk Kum.)*

The authors are with The Cho Chun Shik Graduate School of Green Transportation, Korea Advanced Institute of Science and Technology, Daejeon 34141, South Korea (e-mail: kimjh2608@kaist.ac.kr; dskum@kaist.ac.kr).

Color versions of one or more of the figures in this paper are available online at http://ieeexplore.ieee.org.

Digital Object Identifier 10.1109/TITS.2017.2768318

covers to check whether two trajectories intersect with each other [4]–[6] or comparing intersection times for a give intersection area between two trajectories [7]–[9]. However, this deterministic approach is inherently unable to reflect the uncertainty of the future motion, and collision predictions can completely miss potential risks if the vehicles behave differently than their predicted trajectory. In a similar manner to the deterministic approach, a Monte-Carlo simulation can be applied which randomly generates potential future trajectories based on control input samples. And then, a collision probability can be approximately computed based on the fraction of trajectories that result in collision from among all the generated ones [10], [11].

Note that, these trajectories are commonly generated using a simplified kinematic model, such as CYRA model since the future poses of vehicles can be easily computed by using the analytic solution. However, the prediction performance of the these models quickly deteriorates during highly transient maneuvers, such as lane changes [12]. To overcome this limitation, the maneuver-based trajectory prediction is able to be applied, which firstly estimates a driving maneuver, and then, future trajectories are generated as corresponding to the identified maneuvers. In order to do this, Interacting Multiple Model (IMM) filters are well implemented as the probabilistic model for estimating a multimodal behavior of relevant vehicles [13], [14]. Vehicle maneuvers can also be estimated by evaluating the similarity between the current vehicle motion and the road network, the lane topology [15], [16] or the centerline of driving lanes [31]. Furthermore, the probabilistic inference method such as Hidden Markov Model (HMM) [17], Dynamic Bayesian Networks (DBN) [18], [40], or Artificial Neural Network (ANN) with Support Vector Machine (SVM) [45] is able to be applied for the maneuver recognition based on the observation sequence or training data. The accuracy of driving maneuver prediction can be improved by considering interaction between vehicles based on the machine learning techniques [41] or a game theory [42].

Another approach for risk evaluations is the probabilistic approach, which takes the motion uncertainty into account. This approach introduces error propagation along the predicted trajectory to represent the uncertainty of a future state [19], [20]. The uncertainty is generally modeled by the model-based prediction part of the Kalman filter with a Gaussian distribution. In this approach, collision probability at each prediction time can be calculated by the ratio of poses of vehicles in a collision, which are generated from the Gaussian distribution [2], [21], [22]. Also, the amount of overlap between ellipsoids, defined as a variance of vehicle states, can be used to compute collision probability, which denotes a future state uncertainty [23]. However, the motion uncertainty modeled by the Gaussian distribution does not consider the road geometry or the nature of lane-based driving, and thus cannot properly describe the motion uncertainties that are presented in real-world driving conditions.

Therefore, in this paper, we propose a risk assessment algorithm that can accurately estimate the collision risks over a longer time horizon by applying lane-based probabilistic motion prediction of surrounding vehicles as shown in Fig. 2. In contrast with the existing prediction methods based on the Gaussian distribution, the future motion uncertainty of the proposed method is modeled with respect to lanes, and thus the lane-based model can properly predict the motion uncertainties in real-world driving conditions. In addition, the proposed model can easily handle road geometry and constraints such as the lane number and the road width. In this study, the proposed model is called as the probabilistic target lane model, and it computes probabilities that represent which lane surrounding vehicles are likely to follow in the near future. Using the lane-based probabilistic target lane model, safety measure is estimated by computing the collision risks of local path candidates, which involves the use of both a time-to-collision (TTC) value between two trajectories (ego and surrounding vehicle trajectories) and the probability distribution of each target lane.

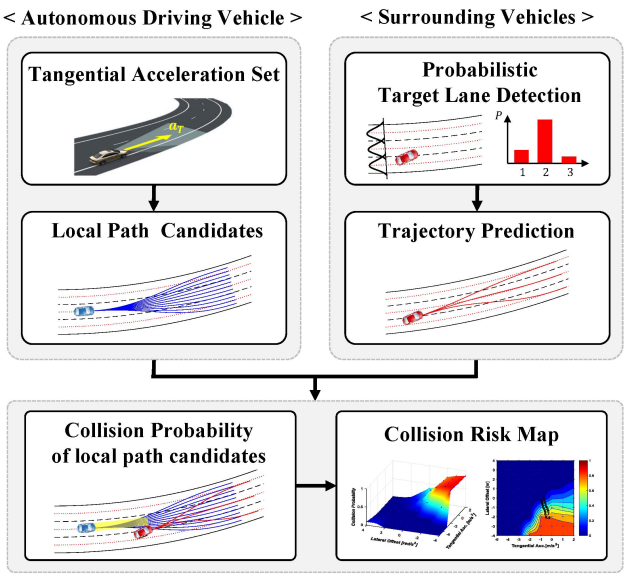

Fig. 2. The overall framework of the proposed risk assessment algorithm.

C. Paper Outline

The remainder of this paper is organized as follows. First, Section II describes the generation of local path candidates for the ego vehicle in curvilinear coordinates. In Section III, the probabilistic motion prediction of surrounding vehicles, which is composed of both the probabilistic target lane detection and trajectory prediction, are explained. In Section IV, we suggest the collision risks of local path candidates for calculating the safety margin. Finally, model validation and driving simulation results are shown in Section V. The performance of the probabilistic target lane detection is analyzed by comparing the maneuver probability derived from the NGSIM trajectory database and computed model probabilities. Also, the proposed algorithm is applied in simulations that rear-end and cut-in driving scenarios with multiple vehicles on a curved road. Conclusions and the future works are discussed in Section VI.

II. Generation of Local Path Candidates

In order to predict a potential collision risk in the near future, local path candidates are generated in the curvilinear coordinates which the ego vehicle can follow inside the road

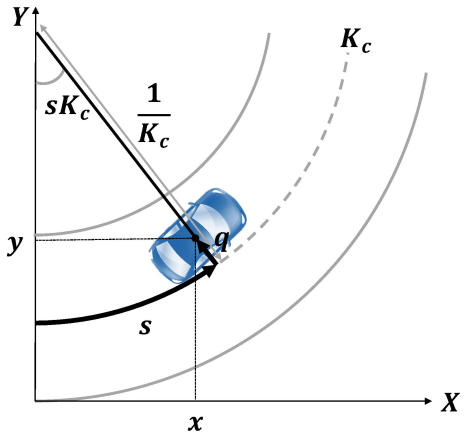

Fig. 3. Relationship between the Cartesian coordinates (x, y) and the curvilinear coordinates (s, q).

boundary. These local path candidates can be immediately employed as the desired control strategy to avoid a collision. That is, in this study, a state space sampling method is adopted for the trajectory generation [24]–[26], because unlike control space sampling, it is suitable for generation of local path candidates that do not violate the road geometry, such as the road width.

A. Curvilinear Coordinates

In this study, local path candidates are generated based on curvilinear coordinates (*s,q*), which allows easy handling of the road curvature, and decouples lateral motion from tangential motion. Therefore, the curvilinear coordinates are more convenient than the Cartesian coordinates when modeling and predicting the vehicle motions on a curved road for real-time implementation [4], [28]. In this coordinates, the horizontal axis is the arc-length s that is the moving distance along the curvature, and the vertical axis is the lateral offset from the road centerline q [27], [28]. The relationship between curvilinear and Cartesian coordinates can be derived as shown in Eq. (1) and Fig. 3.

$$\begin{aligned} x &= \left(\frac{1}{K_c} - q\right) \cdot \sin(sK_c) \\ y &= \frac{1}{K_c} - \left(\frac{1}{K_c} - q\right) \cdot \cos(sK_c) \end{aligned} \tag{1}$$

where K_c is the piecewise constant curvature of the road centerline, and the curvature of local path candidates as in Eq. (2) can be derived from the first and the second derivative of Eq. (1) with respect to time [27].

$$\begin{aligned} k &= \frac{\dot{x}\dot{y} - \ddot{x}\dot{y}}{\left(\dot{x}^2 + \dot{y}^2\right)^{3/2}} \\ &= \frac{S}{Q}\left(K_c + \frac{(1 - qK_c)\left(d^2q/ds^2\right) + K_c(dq/ds)^2}{Q^2}\right) \end{aligned} \tag{2}$$

$$S = sgn(1 - qK_c) \tag{3}$$

$$Q = \sqrt{(dq/ds)^2 + (1 - qK_c)^2} \tag{4}$$

where sgn(·) indicates the sign of a given function. Here, the lateral offset q should become less than the radius of curvature of the road centerline (i.e., $\text{sgn}(1 - qK_c) > 0$) in order to guarantee the kinematical feasibility. Consequently, the feasible local path candidates are generated based on the vehicle model as shown in Eq. (5), which satisfy the non-holonomic constraint of vehicle motion.

$$\begin{aligned} \dot{x} &= v \cdot \cos\theta \\ \dot{y} &= v \cdot \sin\theta \\ \dot{\theta} &= v \cdot k \end{aligned} \tag{5}$$

where (x, y) and θ indicate the vehicle's positon and the heading angle. v and k are the velocity and the curvature of a local path candidate, respectively. Note that the curvature of the trajectory is necessary to be limited by considering the allowable lateral acceleration. Local path candidates in Cartesian coordinates can be computed by numerical integration with respect to the arc-length s by substituting Eq. (2) into the vehicle model in Eq. (5).

B. Quintic Polynomial Trajectories

A quintic polynomial with respect to the arc-length $q(s)$ as shown in Eq. (4) is introduced as a basis function for generating local path candidates. Mathematically, this polynomial is the second differentiable function, which allows to conveniently compute the curvature of all local path candidates using Eq. (2).

$$q(s) = \begin{cases} \sum_{i=0}^{5} a_i s^i & (0 \le s < s_f) \\ q_f & (s \ge s_f) \end{cases} \tag{6}$$

where q_i and q_f are the initial and final lateral offsets from the road centerline with respect to the arc-length s. The boundary conditions that are necessary to determine the coefficients of the lateral offset $q(s)$ are shown in Eq. (7).

$$\begin{aligned} q(0) = q_i \quad \frac{dq(0)}{ds} = \dot{q}_i \quad \frac{d^2q(0)}{ds^2} = \ddot{q}_i \\ q(s_f) = q_f \quad \frac{dq(s_f)}{ds} = 0 \quad \frac{d^2q(0)}{ds^2} = 0 \end{aligned} \tag{7}$$

Here, $\dot{q}$ and $\ddot{q}$ are the lateral velocity and the lateral acceleration in curvilinear coordinates, respectively. s_f is the final arc-length of a local path candidate and we assume the road width is given, which is a constraint of the lateral offset. Since a quintic function is able to cover any initial boundary conditions up to the acceleration values, a sequential continuity between trajectories can be accomplished. In other words, the ego vehicle is capable of reconstructing its avoidance maneuvers during the execution of a certain local path candidate. For instance, previous methods using the cubic polynomial [4], [25] or the sigmoid function [29] cannot meet this requirement. Also, in terms of driving comfort, this function was proved to be optimal trajectory that allowed squared jerk to be minimize in [30]. Here, the longitudinal motion in this coordinate is modeled as the constant acceleration model regarding time by Eq. (8).

$$s_f = v_0 t + \frac{1}{2}at^2 \tag{8}$$

where v_0 is the current tangential velocity and a is the acceleration, which can be employed as the control input.

As a result, since both the lateral offset and tangential acceleration, which represent attempts to change velocity, are considered, all possible maneuvers involving the lane changes or staying in the current lane while accelerating or decelerating can be included in the set of local path candidates.

The initial offset, q_i and the curvature of the road centerline, K_c in Eq. (9) and (10) are calculated by using the parabolic model, $y = c_2x^2 + c_1x + c_0$ [31] for the road centerline.

$$K_c = \frac{d^2y/dx^2}{[1 + (dy/dx)^2]^{3/2}} \tag{9}$$

$$q_i = \sqrt{(x_c - x^*)^2 + (y_c - y^*)^2} \tag{10}$$

where (x_c, y_c) and (x^*, y^*) are the current position of vehicles and the nearest point on the road centerline from the vehicle, respectively. We assume that coefficients of the parabolic model are provided by sensors such as a camera and/or global positioning system. Here, initial offset, q_i denotes the smallest distance between the current position of the ego vehicle and any point on the road centerline. By substituting a parabolic road centerline model into Eq. (9), we can easily find the x_c which minimizes the q_i^2 by differentiating the 4^{th} order polynomial, while also finding the corresponding position (x_c, y_c).

C. Trajectory Plane

In order to provide intuitive risk assessment results, the collision risks of the local path candidates are plotted on a 2-dimensional trajectory plane S_T where each set of the tangential acceleration a and the final lateral offset q_f values represents one of local path candidates as like in Fig. 4 and Eq. (11).

$$S_T = (a_i, q_{f,j}) \quad for\ i \in [1, \cdots, N_{acc}],\ \ j \in [1, \cdots, N_{path}] \tag{11}$$

Each local path candidate of the ego vehicle can be projected as a single point onto the trajectory plane because each of the trajectories has a unique final lateral offset for a given tangential acceleration. A feasible range of tangential acceleration values is determined based on both the vehicle performance and the road surface conditions.

III. Lane-Based Probabilistic Motion Prediction of Surrounding Vehicles

In this section, the uncertain future motions of surrounding vehicles are modeled by using the Interacting Multiple Model (IMM) framework based on the target lane model. Unlike previous methods that simply apply Gaussian distribution over the control input or the position in Cartesian coordinates, the pro- posed method describes uncertain vehicle motions with respect to lanes in curvilinear coordinates, which is more suitable for handling road geometry and constraints. Specifically, the probability that a vehicle is likely to converge to a specified lane in the near future is calculated for each lane from the lateral offset q and lateral velocity $\dot{q}$ in the curvilinear coordinates. Note that these two entities are the most useful features for the maneuver prediction [32]. Finally, the above lane probabilities are respectively assigned

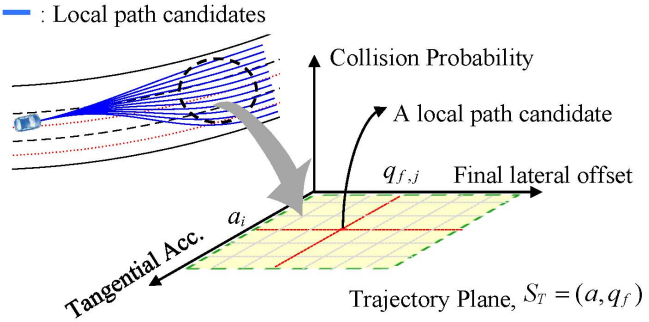

Fig. 4. Trajectory plane where a local path candidate is plotted as a single point for a given set of the tangential acceleration and the final lateral offset.

to the corresponding future trajectories of surrounding vehicles towards the centerline of each lane. The proposed lane-based motion prediction algorithm is described as follows.

A. Probabilistic Target Lane Detection

The design of the probabilistic target lane detection algorithm is based on the Interacting Multiple Model (IMM) framework except for the filtering part. Note that this algorithm mainly aims to model the future motion uncertainty of vehicles rather than estimate the vehicle state. In the literature, the IMM approach has often been implemented for probabilistic maneuver recognition using multiple dynamic models with corresponding model probabilities [13], [32], [44]. The relationships between these dynamic models are described by the Markov Chain, in which the model transitions are dictated by the transition probability matrix (TPM). For example, the lane keeping and the lane change maneuvers are modeled by the constant acceleration (CA) and constant yaw rate and acceleration (CYRA) model, respectively. In this manner, the IMM can predict whether a vehicle intends to keep its current lane or to change lane based on the model probabilities. However, this approach cannot cover all the possible vehicle behaviors because the number of dynamic models is limited. To overcome this problem, the maneuver-based models are replaced with lane-based models in order to predict the future behavior of vehicles in terms of the target lane. Furthermore, a variable (lateral velocity-dependent) TPM is introduced in order to improve the prediction performance of the target lane detection algorithm. The probabilistic target lane detection algorithm, summarized in Fig. 5, consists of two parts, the interaction and the model probability update, for a given TPM.

1) Interaction(Mixing): At the beginning of each time step, the predicted model probability $\mu^j_{k|k-1}$ is calculated by multiplying the model probability in the previous time step μ_{k-1} and the lateral velocity-dependent transition probability $\pi_{ij}(\dot{q})$ from the i^{th} to j^{th} lane as in Eq. (12). Mixed model probability $\mu^{ij}_{k|k-1}$ is computed by dividing each predicted model probability by the total summation of probabilities as in Eq. (13).

$$\mu^j_{k|k-1} = \sum_i \pi_{ij}(\dot{q}_k) \cdot \mu^i_{k-1} \tag{12}$$

$$\mu^{ij}_{k|k-1} = \frac{\pi_{ij}(\dot{q}_k) \cdot \mu^i_{k-1}}{\mu^j_{k|k-1}} \tag{13}$$

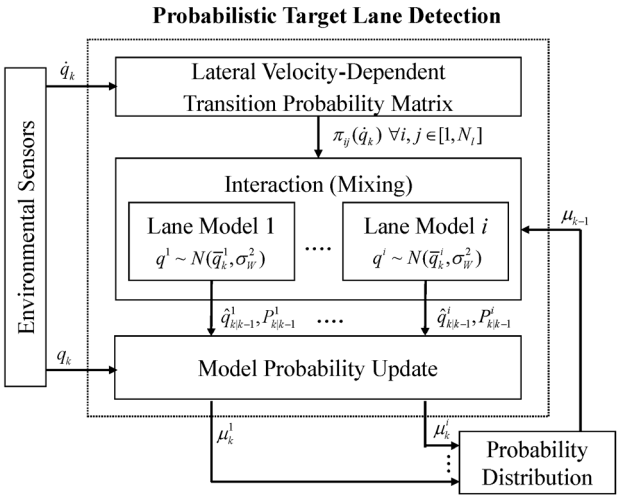

Fig. 5. The flow chart of the probabilistic target lane detection algorithm.

Next, the mixed lateral offset $\hat{q}^j_{k|k-1}$ and its covariance $P^j_{k|k-1}$ are computed as a weighed sum between the mixed model probabilities and the center position of each lane $\bar{q}^i$ in curvilinear coordinates as in Eq. (14) and (15).

$$\hat{q}^j_{k|k-1} = \sum_i \mu^{jj}_{k|k-1} \cdot \bar{q}^i_{k-1} \tag{14}$$

$$P^j_{k|k-1} = \sum_i \mu^{jj}_{k|k-1} \cdot \left[Q^j + \left(\bar{q}^i_{k-1} - \hat{q}^i_{k|k-1} \right) \times \left(\bar{q}^i_{k-1} - \hat{q}^i_{k|k-1} \right)^T \right] \tag{15}$$

Note that the multiple centerline models shown in Fig. 6 are formulated based on a Gaussian distribution with respect to the lateral offset q from the road centerline in Eq. (16).

$$q^i_k = \bar{q}^i_k + Q^i \quad \text{for all } i \in [1, 2, \ldots, N_l] \tag{16}$$

where N_l indicates the total number of lanes on the road. $Q_i \sim N(0, \sigma^2_w)$ represent the zero-mean normal distribution with variance, σ^2_w, which is set as $(W/4)^2$ to cover deviation from the center of the lane by two-sigma variance. Here, W is the width of each lane.

2) Model Probability Update: After the interaction (mixing) step is implemented, each model probability is updated based on the residual term r_k and its covariance S_k at time k, which is the difference between a mixed lateral offset $\hat{q}^j_{k|k-1}$ and an observed lateral offset z_k as in Eq. (17) and (18).

$$r^j_k = z_k - \hat{q}^j_{k|k-1} \quad \text{where } z_k = q_k + R \tag{17}$$

$$S^j_k = P^j_{k|k-1} + R \tag{18}$$

where $R \sim N(0, \sigma^2_q)$ is the zero-mean white Gaussian measurement noise of the lateral offset. We assume that the lateral offset of vehicles with respect to the road centerline is measured from a suitable sensor suite such as a camera, Radar, or Lidar. Also, the likelihood function of the observation Λ_k is assumed to be a Gaussian probability density function (PDF) as shown in Eq. (19). Based on these,

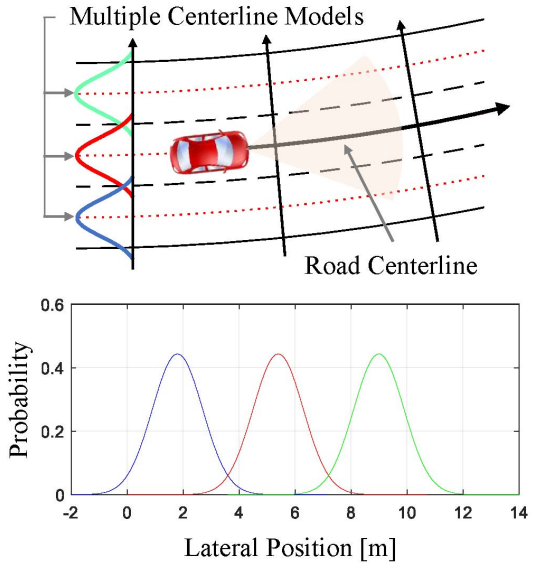

Fig. 6. Multiple centerline models with respect to the lateral offsets in curvilinear coordinates for the case of three lanes on the road.

the model probability for each lane is updated by Eq. (20).

$$\Lambda^j_k = N(r^j_k; 0, S^j_k) = \frac{1}{\sqrt{2\pi S^j_k}} \exp\left[-\frac{\left(r^j_k\right)^2}{2S^j_k} \right] \tag{19}$$

$$\mu^j_k = \frac{\Lambda^j_k \cdot \mu^j_{k|k-1}}{\sum_i \Lambda^i_k \cdot \mu^i_{k|k-1}} \tag{20}$$

B. Lateral Velocity-Dependent Transition Probability Matrix

In practice, the IMM approach often adopts the constant transition probability matrix (TPM) based on the Markovian assumption. However, when a time-invariant TPM is utilized for the target lane detection algorithm, the lane change maneuver cannot be rapidly detected and the maneuver recognition performance may not be acceptable. Thus, it is essential to design the conditional transition probability modeled as a function of continuous state variables [34]. From this point of view, the lateral velocity-dependent transition probability $\pi_{ij}(\dot{q})$, described in Eq. (21), is proposed and illustrated in Fig. 7.

$$\pi_{ij}(\dot{q}_k) = P\left[L_k = j | L_{k-1} = i, \dot{q}_k \right] \quad \text{where } \sum\nolimits_i \pi_{ij} = 1 \tag{21}$$

where $\dot{q}_k$ is the lateral velocity of a surrounding vehicle in the curvilinear coordinates, and i and j indicate the i^{th} and j^{th} lane, respectively. $L_k \in [1, 2, \ldots, N_l]$ indicates the state of the target lane where a vehicle is likely to move at time k. This conditional transition probability allows the lane transition to be detected earlier than the model using the constant transition probability. Eq. (21) is formulated as the Gaussian cumulative distribution function (CDF) to represent stochastic inequality transition conditions [34]. In other words, the transition criteria λ_{ij} from the i^{th} to the j^{th} lane is defined

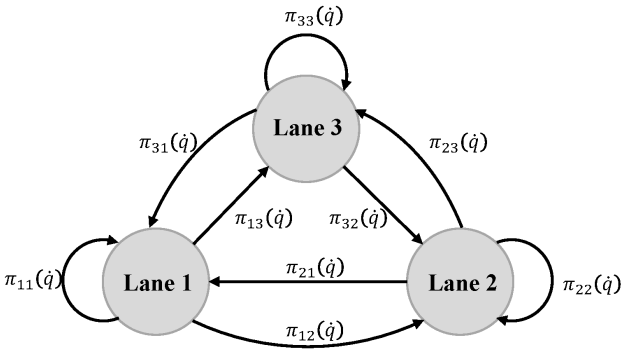

Fig. 7. The representation of the lateral velocity-dependent transition probability matrix in case of the three lane on the road.

as a random variable, which follows the Gaussian PDF as in Eq. (22).

$$\begin{aligned} &\dot{q}_k - \lambda_{ij} \le 0 (i \ge j) \\ &\dot{q}_k - \lambda_{ij} > 0 (i < j) \quad \text{where } \lambda_{ij} \sim N(\rho_{ij}, \sigma_{ij}^2) \end{aligned} \tag{22}$$

where the subscripts i and j indicate the lane numbers assigned from the left-side of the road, consecutively. ρ and σ^2 are the mean and covariance of the transition criteria. From Eq. (21) and (22), the lateral velocity-dependent transition probability is calculated as follows.

$$\pi_{ij}(\dot{q}_k) = \frac{\pi_{0,ij}(\dot{q}_k)}{\sum_j \pi_{0,ij}(\dot{q}_k)} \tag{23}$$

$$\pi_{0,ij}(\dot{q}_k) = \begin{cases} \pi_{ij}^{ini} + \Phi(\dot{q}_k; \rho_{ij}, \sigma_{v,ij}^2) & (\dot{q}_k - \rho_{ij} \le 0) \\ \pi_{ij}^{ini} + \left[1 - \Phi(\dot{q}_k; \rho_{ij}, \sigma_{v,ij}^2)\right] & (\dot{q}_k - \rho_{ij} > 0) \end{cases} \tag{24}$$

where π_{ij}^{ini} is the initial transition probability. Note that each a priori transition probability, $\pi_{0,ij}(\dot{q})$, is divided by the total summation of it in order to make the probability of the whole set equals to one. $\Phi(x; \rho, \sigma_v^2)$ denotes the Gaussian CDF with the mean ρ and variance σ_v^2 as in Eq. (25).

$$\Phi(x; \rho, \sigma_v^2) = \int_{-\infty}^{x} \frac{1}{\sigma_v^2 \sqrt{2\pi}} \exp\left\{-\frac{(x-\rho)^2}{2\sigma_v^2}\right\} dx \tag{25}$$

where σ_v^2 is equal to the summation of σ_T^2 and $\sigma_{\dot{q}}^2$. σ_T^2 and $\sigma_{\dot{q}}^2$ denote the predetermined variance of the stochastic transition conditions and the lateral velocity measurement, respectively. Note that ρ and σ_T^2 for the stochastic transition conditions are design parameters and are obtained from the NGSIM database, which is discussed in Section V.

C. Trajectory Prediction of Surrounding Vehicles

After the model probability distribution of lanes has been calculated, future trajectories of a surrounding vehicle are generated towards the centerline of each lane. Then, those probabilities are assigned to the corresponding future trajectories as shown in Fig. 8. Trajectories are generated by using a cubic polynomial as a basis function in the curvilinear coordinates as in Eq. (26). The boundary conditions to determine the coefficients of this polynomial are listed in Eq. (27).

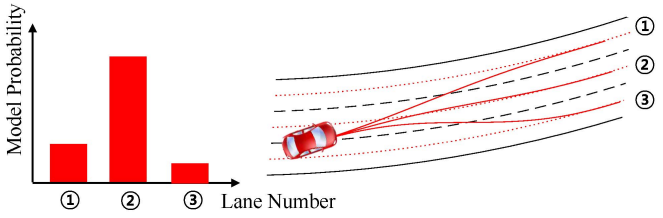

Fig. 8. Trajectory prediction of a surrounding vehicle with corresponding model probabilities of road lanes.

$$q(s) = \begin{cases} \sum_{i=0}^{3} a_i s^i & (0 \le s < s_f) \\ q_f & (s \ge s_f) \end{cases} \tag{26}$$

$$\begin{aligned} &q(0) = q_i \quad \frac{dq(0)}{ds} = \tan\psi \\ &q(s_f) = q_f \quad \frac{dq(s_f)}{ds} = 0 \end{aligned} \tag{27}$$

where ψ is the heading angle with respect to the tangential line to the road centerline. q_i and q_f^c are the current lateral offset of a surrounding vehicle and the center position of each lane from the road centerline, respectively. Note that the cubic polynomial is adopted as the basis function rather than the quintic function for local path candidates. The cubic polynomial is selected because the lane change trajectories with large lateral velocity values tend to show overshoot and/or oscillation due to the nature of the quintic function. The arc-length representing the distance moved along predicted trajectories is modeled as a constant acceleration model regarding time as like that of the ego vehicle.

IV. Risk Assessment of Local Path Candidates

In this section, the collision risk of a local path candidate is computed by incorporating both the time-to-collision (TTC) for a pair of trajectories, and the model probabilities of each lane. These collision risk values are projected onto the trajectory plane where each set of the tangential acceleration and the final lateral offset indicates a single local path candidate, as discussed in Section II.C. This collision risk map provides intuitive risk information, which can be used for path planning and control strategy in order to avoid or mitigate a collision.

A. Computation of Time-to-Collision

In Sections II and III, both the local path candidates of the ego-vehicle and the future trajectories of surrounding vehicles are generated. Based on these trajectories, the time-to-collision (TTC) is computed by checking whether two vehicle's rectangular shapes overlap each other by utilizing the separating axis theorem. The separating axis theorem [35] is a useful tool for collision detection because it considers the geometry of the vehicle. If there exists a separating axis that completely divides these two polygons, it represents that two convex polygons such as rectangles do not intersect. This is illustrated in Fig. 9. At time t_1 within the prediction time horizon [0, T_p], the rectangles of two vehicles do not overlap because a separating axis exists, and thus, t_1 is not a time-to-collision. On the other hand, t_2 is confirmed as the time-to-collision because two vehicles' rectangular shapes overlap

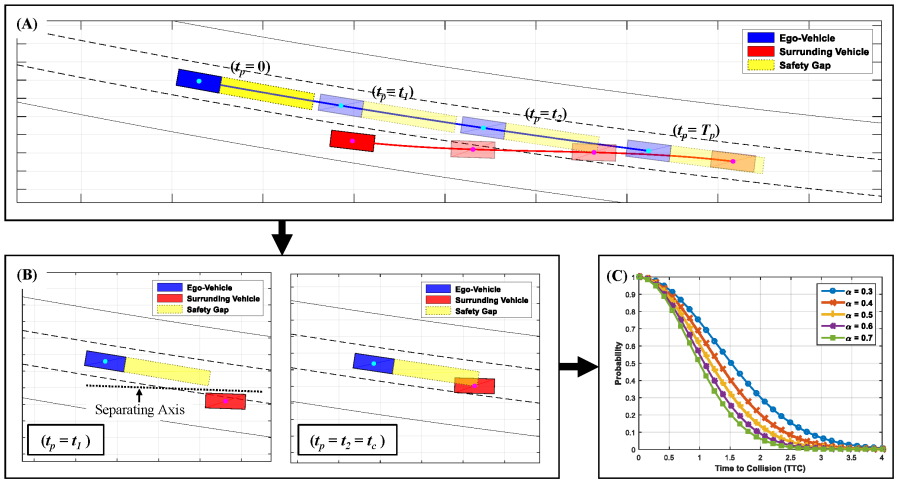

Fig. 9. (A) Computation of TTC between each pair of trajectories by applying the separating axis theorem at discrete time steps (B) TTC is confirmed as t_2 since two vehicles' rectangular shape firstly overlap. (C) TTC is converted as a collision risk value following an exponential function with rate of risk regarding time.

for the first time at this time along the predicted trajectories. Note that when both the relative velocity and headway distance are small, TTC would be high, which may be considered safe. However, in reality, the potential collision risk is quite high due to the short headway distance. To prevent such misjudgments, a safety range s_{safe} with a constant time headway is added in front of the ego vehicle as shown in Fig. 9 (A) and Eq. (28).

$$s_{safe} = s_0 + v \cdot T_{head} \tag{28}$$

where v is the current velocity of the ego vehicle. s_0 and T_{head} are the minimum safety gap and the time-headway, respectively.

B. Collision Risk of Local Path Candidates

The most popular approach for estimating collision probability is the Monte-Carlo simulation. This method computes the fraction of samples in a collision that are randomly generated from a set of potential trajectories or poses of vehicles such as the position and the heading. Unfortunately, this approach requires a high computational load because the probability needs to be computed in an iterative manner with a significant number of samples to obtain reliable results. In contrast, in this paper, the time-to-collision (TTC) t_c between a pair of a local path candidate T_E and a predicted trajectory of an i^{th} surrounding vehicle T_{Si} is heuristically converted into a collision risk metric by using an exponential function [36] as in Eq. (29) and Fig. 9 (C).

$$P\left(C_{S_i} \middle| T_E, T_{S_i}\right) = \begin{cases} \exp(-\alpha t_c^2) & (\exists t_c, v_E(t_c) \cap v_{S_i}(t_c) \neq \emptyset) \\ 0 & \text{otherwise} \end{cases} \tag{29}$$

where α is the rate of collision risk depending on a time-to-collision t_c. Note that this tunable parameter can be adjusted when a designer wants to set the collision risk higher or lower for a given level of a time-to-collision depending on the various local driving style. For example, as shown in Fig. 9(C), collision risk rises earlier at higher TTC value for low α value but rises later at lower TTC value when α value is high. V_E and V_s indicate the rectangular shape of the ego vehicle and a surrounding vehicle, respectively. Then, a collision risk of local path candidates T_E with an i^{th} surrounding vehicle $P(C_{Si}|T_E)$ is computed by considering the model probability of each lane as in Eq. (30).

$$P(C_{S_i} | T_E) = \sum_{j=1}^{N_l} P\left(C_{S_i} \middle| T_E, T_{S_i}(l)\right) \cdot P\left(T_{S_i}(l = j)\right) \tag{30}$$

where j is a specific lane number on the road and $P(T_{Si}(l))$ indicates the model probability of a corresponding lane l for an i^{th} surrounding vehicle. Finally, the collision risk of local path candidates for multiple vehicle scenarios can be calculated by Eq. (31) [37], [38].

$$P(C|T_E) = \bigcup_{i=1}^{N_S} P\left(C_{S_i} \middle| T_E\right) = 1 - \prod_{i=1}^{N_S} \left(1 - P\left(C_{S_i} \middle| T_E\right)\right) \tag{31}$$

where N_s is the number of surrounding vehicles. For simplicity, we assume that the surrounding vehicles move independently while following their predicted trajectories. This value represents the possibility that a collision occurs with one of surrounding vehicles when the ego vehicle moves along to a specific local path candidate.

V. Simulation Results

In this section, the prediction performance of the lane-based probabilistic model is first validated by comparing the model probabilities from the probabilistic target lane detection algorithm against the maneuver probabilities obtained from real-world traffic data, the NGSIM database. Moreover, in order to verify and demonstrate the effectiveness of the proposed risk assessment algorithm, driving simulations are carried out for two scenarios, rear-end and cut-in, where multiple surrounding vehicles are driving on a curved highway.

A. Next Generation Simulation (NGSIM) Database

The NGSIM database is widely used for the calibration and validation of existing traffic simulation models [39]. The

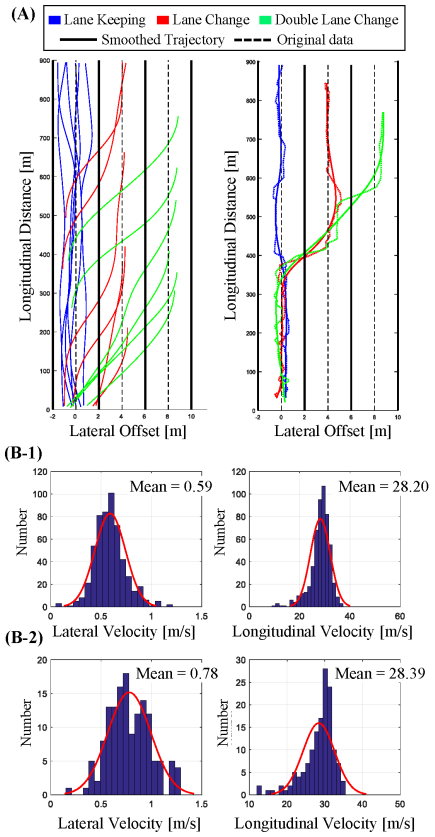

Fig. 10. (A) Smoothed trajectories classified by driving maneuvers (left) and pre-processing result by applying cubic spline smoothing to original data for noise reduction (right). (B-1) and (B-2) are the distribution of the lateral and longitudinal velocity of the smooth trajectories, respectively.

traffic flow data was collected using several video cameras mounted on top of a building located in the middle of the study area, and the trajectory dataset was reconstructed by using image processing techniques. Here, among the four datasets in the original database we choose the prototype dataset for Interstate 80 in the San Francisco bay, California. Note that this dataset was collected on a straight highway with approximately 500 meters in length and consisted of one on-ramp and six freeway lanes. Before any analysis, data preprocessing is necessary due to the noises presented in the raw trajectory data. For noise reduction, cubic spline smoothing is applied to smooth the original data. The distribution of the longitudinal and lateral velocity of the vehicles, computed by numerical difference, is shown in Fig. 10(B).

B. Target-Lane Prediction Model Validation

In order to obtain the maneuver probabilities from the NGSIM database, each trajectory is classified by three maneuvers; lane keeping, lane-change, and double lane-change. Then, these trajectories are categorized by both the lateral offset and the lateral velocity in order to identify whether maneuvers exist in segments s, which consist of the above two quantities. To do this, each trajectory is assigned a value 0 or 1 depending on whether it exists in every segment s, and then, the number of these are counted as like Eq. (32), (33), and Fig. 11(A).

TABLE I

TWO-DIMENSIONAL CORRELATION COEFFICIENT BETWEEN THE MANEUVER AND MODEL PROBABILITY DISTRIBUTION

Driving Maneuvers	2D Correlation Coefficient
Lane Keeping	0.9068
Single Lane Change	0.9024
Double Lane Change	0.9228

$$N_{ij}(T_m) = \sum_{i=1}^{N_i}\sum_{j=1}^{N_j} \Gamma\left(s_i(q), s_j(\dot{q})\right) \tag{32}$$

$$\Gamma\left(s_i(q), s_j(\dot{q})\right) = \begin{cases} 1 & \left(T_m \in \left[s_i(q), s_j(\dot{q})\right]\right) \\ 0 & \left(T_m \notin \left[s_i(q), s_j(\dot{q})\right]\right) \end{cases} \tag{33}$$

where $s(q)$ and $s(\dot{q})$ indicate each segment over the range of the lateral offset, q and lateral velocity, $\dot{q}$ respectively. T_m is a smoothed trajectory categorized by the driving maneuver, m among $M \in$ {Lane keeping, Lane change, Double lane change}. And $\Gamma(\cdot)$ refers to the binary indicator function for checking the existence of a trajectory on a specific segment. And then, the maneuver probabilities can be calculated as shown in Eq. (34).

$$P_{ij}^{m}(s_i(q), s_j(\dot{q})) = \frac{N_{ij}(T_m)}{\sum_{m\in M} N_{ij}(T_m)} \tag{34}$$

The target lane prediction model can be validated by comparing the model probabilities of the proposed algorithm against the maneuver probabilities obtained from the NGSIM database. For a more quantitative and systematic comparison, the two-dimensional correlation coefficients between the two probability distributions are computed. The results confirm that their similarity metrics are high, 0.9 or above, and are summarized in Table I. The error contour between two probabilities are plotted in Fig. 11(B-1∼3) according as three maneuvers. The minimal discrepancy shown in these contour maps also confirm that the model probability maps match the statistical data obtained from real-world traffic. However, the discrepancy is significant at the lower left corner of the first contour in Fig.11(B-1). This shows that the lane-keeping prediction performance of the target-lane detection algorithm hesitates when the lateral offset is small but lateral velocity is high. The main reason for this error comes from the fact that the model probabilities are mainly determined by the lateral offset, while the lateral velocity of vehicles in the transition probability matrix is an auxiliary feature to promote the detectability of the lane change intention. In other words, the IMM-based algorithm inherently has difficulty in predicting lane-keeping maneuver for low lateral offset with high lateral velocity.

Note that the validation result is derived from the following parameters. First, the initial probability distribution μ_0 is set uniformly over the lanes (i.e., $[1/31/31/3]^{\mathrm{T}}$). The initial

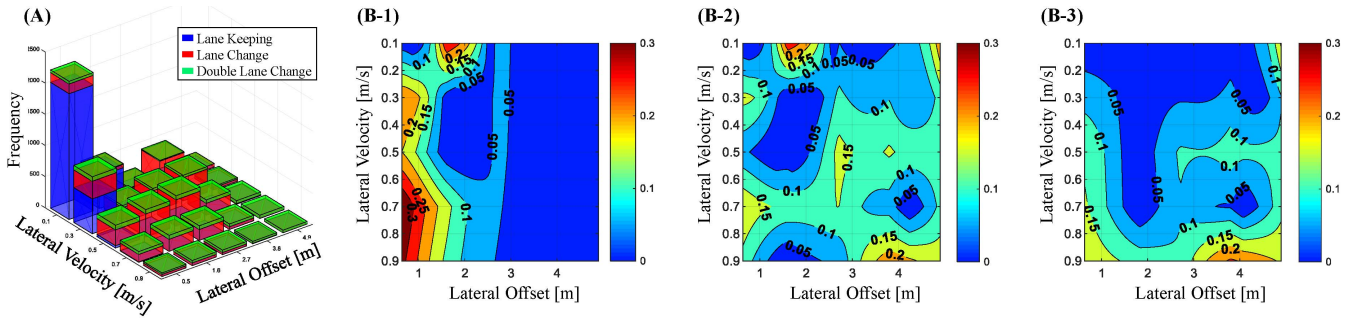

Fig. 11. (A) The number of trajectories depending on maneuvers over the range of lateral offsets and lateral velocities obtained from the NGSIM database (B-1∼3) Error contours between three maneuver probabilities derived from NGSIM database and model probabilities computed from the probabilistic target lane detection; (B-1) Lane keeping, (B-2) Lane change, and (B-3) Double lane change, respectively.

TABLE II
SIMULATION PARAMETERS

Symbol	Description	Unit	Value
L_f	Distance from the center of gravity to front	m	2.4
L_r	Distance from the center of gravity to rear	m	2
T_w	Width of the vehicles	m	1.8
W	Width of the lanes on the road	m	4
N_l	Number of the lanes on the road	·	3
a_{set}	Tangential acceleration set of the ego vehicle	m/s^2	[-5,2]
α	Rate of collision risk with respect to the TTC	·	0.5
T_p	Prediction time horizon	sec	3

transition probability matrix, π_{ij}^{ini} is defined as Eq. (35).

$$\pi_{ij}^{ini} = \begin{bmatrix} 0.94 & 0.05 & 0.01 \\ 0.05 & 0.89 & 0.05 \\ 0.01 & 0.05 & 0.94 \end{bmatrix} \tag{35}$$

Also, the means and the covariance of the stochastic transition conditions $\lambda \sim N(\rho, \sigma_v^2)$ in terms of the lateral velocity are acquired from the distribution of the lateral velocity over the smoothed trajectories. The parameters specified for the stochastic transition conditions are shown in Eq. (36) subject to the single or double lane change maneuvers, respectively.

$$\begin{aligned} \rho_{ij} &= \text{sgn}(i-j)\cdot 0.42, \quad \sigma_{ij}^2 = (0.15)^2 \text{ for } |i-j| = 1 \\ \rho_{ij} &= \text{sgn}(i-j)\cdot 0.90, \quad \sigma_{ij}^2 = (0.22)^2 \text{ for } |i-j| = 2 \end{aligned} \tag{36}$$

where i, $j \leq N_l$ are lane numbers assigned from the left-side of the road consecutively and sgn$(\cdot)$ is the sign of a given function.

C. Driving Simulation

In order to demonstrate the effectiveness of the target-lane prediction and risk assessment algorithms, driving simulations are carried out for two scenarios, rear-end and cut-in, where multiple surrounding vehicles are driving on a curved highway. The simulation parameters are summarized in Table II. The vehicle dimensions of both the ego vehicle and the surrounding vehicle are assumed to be identical in this simulation, and the initial tangential velocities of all the vehicles are set to 20m/s (≈ 70km/h). Also, a set of the tangential acceleration is selected based on the maximum acceleration and deceleration performance of the ego vehicle. A set of the lateral offset is determined with respect to the road centerline while bounded in a road width.

1) Preceding Vehicle Braking Scenario: The first scenario is that a vehicle in front of the ego vehicle gradually decelerates in the same lane. Additionally, in order to make the scenario more interesting and realistic, a vehicle (1) driving at higher speed than that of the ego vehicle is driving in the left lane, and a vehicle (3), driving in the right lane, simultaneously initiates a lane change towards the ego vehicle's lane. Here, the yellow region denotes the minimum safety range, and solid blue lines represent a set of local path candidates with zero tangential acceleration at each time step. Fig. 12 illustrates that the probability distribution changes while vehicle (3) changes its lane, and thus, the target-lane prediction algorithm is working properly. Furthermore, the collision risk maps, the right-most figures in Fig. 12, indicates that the collision risks of the local path candidates with high acceleration increases with time due to the braking preceding vehicle. In addition, significant collision risks can be observed when the ego vehicle performs a left lane change with hard deceleration because vehicle (1) is driving faster than the ego vehicle. However, if vehicle (2) approaches in closer proximity to the ego vehicle than that shown in Fig. 12(C), a significant deceleration or right lane change would be required to avoid a collision. In the case of vehicle (3), it does not contribute much to collision risks even though it is moving into the ego vehicle's lane. This is because the arrival and departure time at the potential conflict area do not overlap within the prediction time horizon. In other words, a collision will not occur because one vehicle exits the intersection area before the other vehicle arrives.

2) Cut-in Scenario: The second scenario involves a vehicle driving in the right-side lane which cuts in front of the ego vehicle, and thus the distance gap between the ego vehicle and the closest-preceding-vehicle abruptly drops below a minimum safety gap. In Fig. 13, the collision risk map illustrates that the collision risks of the local path candidates towards the third lane rapidly increases because the intention of vehicle (3) to change target lane is detected. This recognition can be seen from two probability (middle) plots in Fig. 13 where the model probability of the second lane for vehicle (3) gradually increases whereas that of the third lane declines

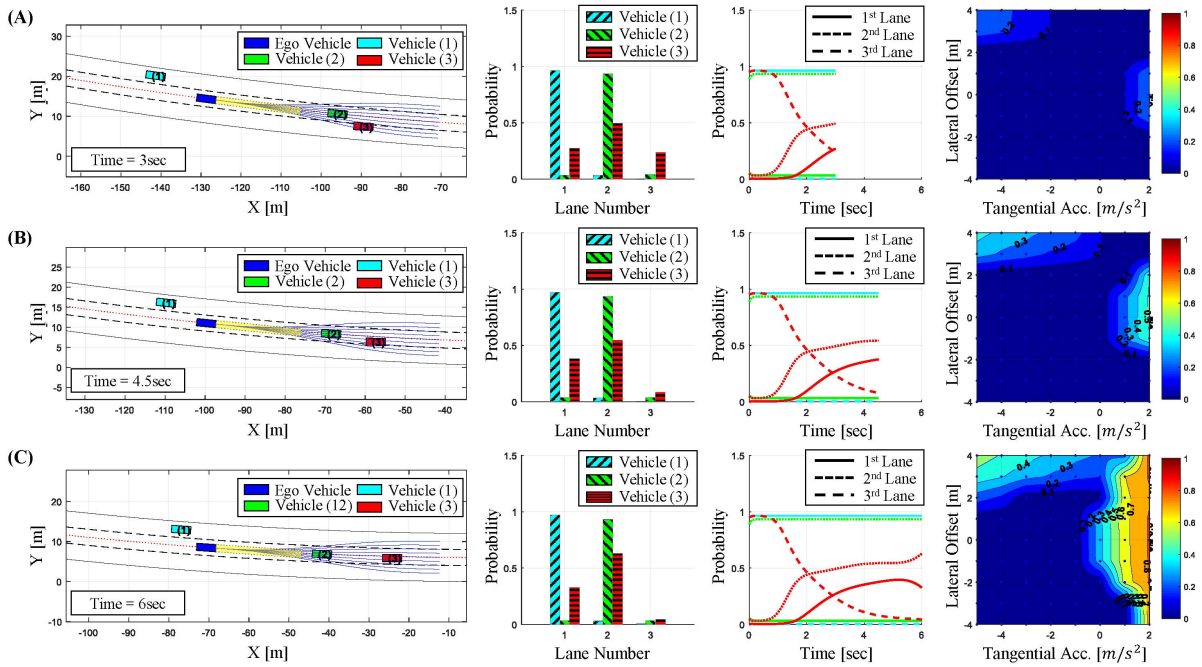

Fig. 12. Simulation result of preceding vehicle braking scenario (A) $t = 3$ sec, (B) $t = 4.5$ sec, (C) $t = 6$ sec.

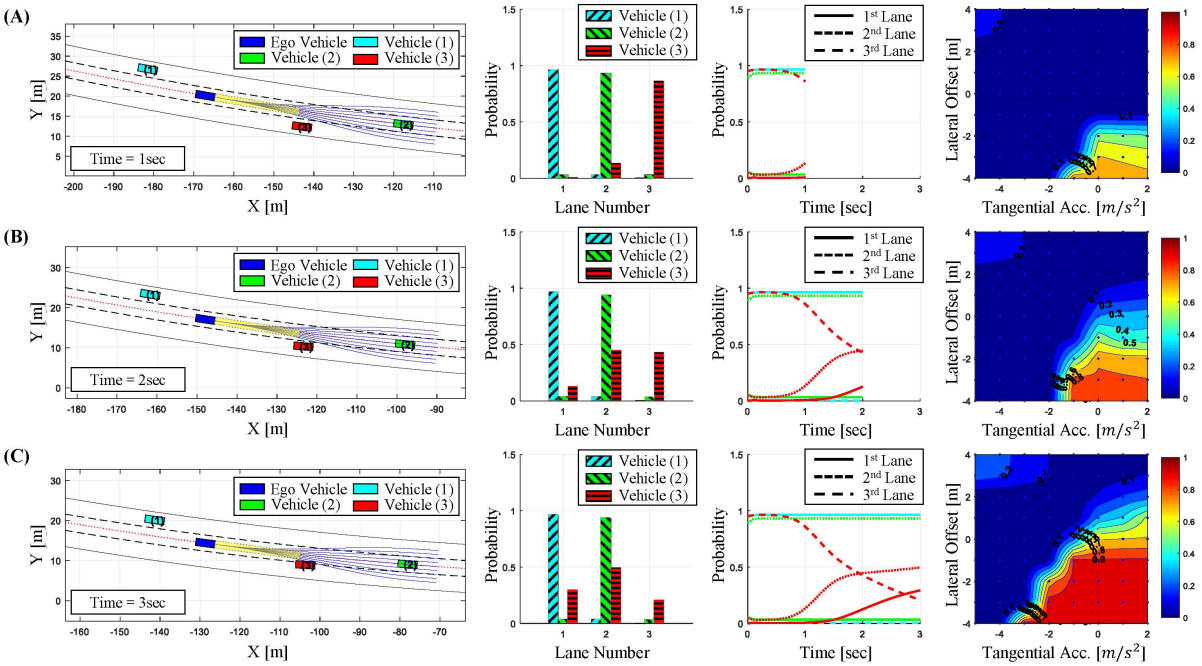

Fig. 13. Simulation result of cut-in scenario (A) t = 1 sec, (B) t = 2 sec, (C) t = 3 sec.

simultaneously. In addition, since vehicle (1) in the first lane is driving faster than the ego vehicle, the collision risks of the local path candidates towards the left lane with hard braking also increase. In summary, the collision risk map suggests that there are three options for the ego vehicle to prevent or mitigate collision; 1) stay in the lane while braking, 2) change lanes toward the right-side while braking, and 3) change lanes towards the left-lane while accelerating.

VI. Conclusions and Future Works

In this paper, we propose a risk assessment algorithm that accurately computes the collision risks for a set of local path candidates along with the lane-based probabilistic motion prediction of surrounding vehicles. The proposed algorithm provides long-term risk predictions based on probabilistic target lane predictions, and this provides the ego vehicle with sufficient time to respond to many complex hazardous situations. This risk assessment algorithm can estimate future risks associated with surrounding vehicles for driver assistance systems, and enables autonomous vehicles to safely cope with dangerous driving situations. In particular, by modeling the future motion uncertainty in the context of road lanes, the algorithm is able to naturally take road geometry into consideration.

However, the predictability of a lane change could be improved for the low lateral offset region. Furthermore, the proposed approach does not consider interactions with surrounding vehicles when a control strategy is considered in the loop. Therefore, in the future, interactions between vehicles will be considered for both motion and risk predictions, and close the loop with a control strategy. In addition, experimental tests will be conducted to validate and evaluate the prediction performance of the algorithm.

REFERENCES

[1] J. Ziegler *et al.*, "Making bertha drive—An autonomous journey on a historic route," *IEEE Intell. Transp. Syst. Mag.*, vol. 6, no. 2, pp. 8–20, Feb. 2014.

[2] J. Huang and H.-S. Tan, "DGPS-based vehicle-to-vehicle cooperative collision warning: Engineering feasibility viewpoints," *IEEE Trans. Intell. Transp. Syst.*, vol. 7, no. 4, pp. 415–428, Dec. 2006.

[3] J. Hillenbrand, A. M. Spieker, and K. Kroschel, "A multilevel collision mitigation approach—Its situation assessment, decision making, and performance tradeoffs," *IEEE Trans. Intell. Transp. Syst.*, vol. 7, no. 4, pp. 528–540, Dec. 2006.

[4] K. Chu, M. Lee, and M. Sunwoo, "Local path planning for off-road autonomous driving with avoidance of static obstacles," *IEEE Trans. Intell. Transp. Syst.*, vol. 13, no. 4, pp. 1599–1616, Dec. 2012.

[5] N. Kaempchen, B. Schiele, and K. Dietmayer, "Situation assessment of an autonomous emergency brake for arbitrary vehicle-to-vehicle collision scenarios," *IEEE Trans. Intell. Transp. Syst.*, vol. 10, no. 4, pp. 678–687, Dec. 2009.

[6] D. Ferguson, M. Darms, C. Urmson, and S. Kolski, "Detection, prediction, and avoidance of dynamic obstacles in urban environments," in *Proc. IEEE Intell. Veh. Symp.*, Jun. 2008, pp. 1149–1154.

[7] S. Joerer, M. Segata, B. Bloessl, R. L. Cigno, C. Sommer, and F. Dressler, "To crash or not to crash: Estimating its likelihood and potentials of beacon-based IVC systems," in *Proc. 4th IEEE Veh. Netw. Conf.*, Nov. 2012, pp. 25–32.

[8] D. Greene *et al.*, "An efficient computational architecture for a collision early-warning system for vehicles, pedestrians, and bicyclists," *IEEE Trans. Intell. Transp. Syst.*, vol. 12, no. 4, pp. 942–953, Dec. 2011.

[9] J.-H. Kim and D.-S. Kum, "Threat prediction algorithm based on local path candidates and surrounding vehicle trajectory predictions for automated driving vehicles," in *Proc. IEEE Intell. Veh. Symp.*, Jul. 2015, pp. 1220–1225.

[10] A. Eidehall and L. Petersson, "Statistical threat assessment for general road scenes using Monte Carlo sampling," *IEEE Trans. Intell.Transp. Syst.*, vol. 9, no. 1, pp. 137–147, Jan. 2008.

[11] S. Joerer, M. Segata, B. Bloessl, R. Lo Cigno, C. Sommer, and F. Dressler, "A vehicular networking perspective on estimating vehicle collision probability at intersections," *IEEE Trans. Veh. Technol.*, vol. 63, no. 4, pp. 1802–1812, May 2014.

[12] W. Yao, H. Zhao, P. Bonnifait, and H. Zha, "Lane change trajectory prediction by using recorded human driving data," in *Proc. IEEE Intell. Veh. Symp.*, Jun. 2013, pp. 430–436.

[13] R. Toledo-Moreo and M. A. Zamora-Izquierdo, "IMM-based lane-change prediction in highways with low-cost GPS/INS," *IEEE Trans. Intell. Transp. Syst.*, vol. 10, no. 1, pp. 180–185, Mar. 2009.

[14] B. Kim, K. Yi, H.-J. Yoo, H.-J. Chong, and B. Ko, "An IMM/EKF approach for enhanced multitarget state estimation for application to integrated risk management system," *IEEE Trans. Veh. Technol.*, vol. 64, no. 3, pp. 876–889, Mar. 2015.

[15] D. Petrich, T. Dang, D. Kasper, G. Breuel, and C. Stiller, "Map-based long term motion prediction for vehicles in traffic environments," in *Proc. IEEE Conf. Intell. Transp. Syst.*, Oct. 2013, pp. 2166–2172.

[16] J. Wiest, M. Karg, F. Kunz, S. Reuter, U. Krebel, and K. Dietmayer, "A probabilistic maneuver prediction framework for self-learning vehicles with application to intersections," in *Proc. IEEE Intell. Veh. Symp.*, Jul. 2015, pp. 349–355.

[17] J. Firl and Q. Tran, "Probabilistic maneuver prediction in traffic scenarios," in *Proc. Eur. Conf. Mob. Robot.*, pp. 1–6, 2011.

[18] D. Kasper *et al.*, "Object-oriented Bayesian networks for detection of lane change maneuvers," *IEEE Intell. Transp. Syst. Mag.*, vol. 19, no. 3, pp. 19–31, Mar. 2012.

[19] G. R. de Campos, A. H. Runarsson, F. Granum, P. Falcone, and K. Alenljung, "Collision Avoidance at intersections: A probabilistic threat-assessment and decision-making system for safety interventions," in *Proc. IEEE Int. Conf. Intell. Transp. Syst.*, Oct. 2014, pp. 649–654.

[20] B. Kim and K. Yi, "Probabilistic and holistic prediction of vehicle states using sensor fusion for application to integrated vehicle safety systems," *IEEE Trans. Intell. Transp. Syst.* , vol. 15, no. 5, pp. 2178–2190, May 2014.

[21] A. Lambert, D. Gruyer, and G. S. Pierre, "A fast Monte Carlo algorithm for collision probability estimation," in *Proc. 10th Int. Conf. Control, Autom., Robot., Vis. (ICARCV)*, Dec. 2008, pp. 406–411.

[22] S. Ammoun and F. Nashashibi, "Real time trajectory prediction for collision risk estimation between vehicles," in *Proc. IEEE Int. Conf. Intell. Comput. Commun. Process.*, Aug. 2009, pp. 417–422.

[23] A. Houenou, P. Bonnifait, and V. Cherfaoui, "Risk assessment for collision avoidance systems," in *Proc. IEEE Int. Conf. Intell. Transp. Syst.*, Oct. 2014, pp. 386–391.

[24] T. Howard and C. Green, "State space sampling of feasible motions for high?performance mobile robot navigation in complex environments," *J. Field Robot.*, vol. 25, no. 1, pp. 325–345, 2008.

[25] X. Li, Z. Sun, Z. He, Q. Zhu, and D. Liu, "A practical trajectory planning framework for autonomous ground vehicles driving in urban environments," in *Proc. IEEE Intell. Veh. Symp.*, Jun. 2015, pp. 1160–1166.

[26] X. Li, Z. Sun, A. Kurt, and Q. Zhu, "A sampling-based local trajectory planner for autonomous driving along a reference path," in *Proc. IEEE Intell. Veh. Symp.*, Jun. 2014, pp. 376–381.

[27] T. D. Barfoot and C. M. Clark, "Motion planning for formations of mobile robots," *J. Robot. Auton. Syst.*, vol. 46, no. 2, pp. 65–78, 2004.

[28] J. Kim, K. Jo, W. Lim, M. Lee, and M. Sunwoo, "Curvilinear-coordinate-based object and situation assessment for highly automated vehicles," *IEEE Trans. Intell. Transp. Syst.*, vol. 16, no. 3, pp. 1559–1575, Jun. 2015.

[29] M. Knoop and T. Haeussler, "Method for determining an evasion trajectory for a motor vehicle, and safety device or safety system," U.S. Patent 0 067 252 A1, Mar. 6, 2014.

[30] M. Werling, S. Kammel, J. Ziegler, and L. Groll, "Optimal trajectories for time-critical street scenarios using discretized terminal manifolds," *Int. J. Robot. Res.*, vol. 31, no. 3, pp. 346–359, Mar. 2012.

[31] A. Houenou, P. Bonnifait, V. Cherfaoui, and W. Yao, "Vehicle trajectory prediction based on motion model and maneuver recognition," in *Proc. IEEE/RSJ Int. Conf. Intell. Robot. Syst.*, Nov. 2013, pp. 4363–4369.

[32] J. Schlechtriemen, A. Wedel, J. Hillenbrand, G. Breuel, and K.-D. Kuhnert, "A lane change detection approach using feature ranking with maximized predictive power," in *Proc. IEEE Intell. Veh. Symp.*, Jun. 2014, pp. 108–114.

[33] T. Zhou, M. Li, X. Mai, Q. Wang, F. Liu, and Q. Li, "Trajectory generation model-based IMM tracking for safe driving in intersection scenario," *Int. J. Veh. Technol.*, vol. 2011, Nov. 2010, Art. no. 103696.

[34] C. E. Seah and I. Hwang, "State estimation for stochastic linear hybrid systems with continuous-state-dependent transitions: An IMM approach," *IEEE Trans. Aerosp. Electron. Syst.*, vol. 45, no. 1, pp. 376–392, Jan. 2009.

[35] J. Huynh. (2009). *Separating Axis Theorem for Oriented Bounding Boxes*. [Online]. Available: www.jkh.me/files/

[36] C. Tay, "Analysis of dynamic scenes: Application to driving assistance," Ph.D. dissertation, Dept. Comput. Sci., Grenoble Inst. Technol., Grenoble, France, 2009.

[37] D. Althoff, "Safety assessment for motion planning in uncertain and dynamic environments," Ph.D. dissertation, Dept. Elect. Comput. Eng., Tech. Univ. Munich, Munich, Germany, 2013.

[38] M. Schreier, V. Willert, and J. Adamy, "Bayesian, maneuver-based, long-term trajectory prediction and criticality assessment for driver assistance systems," in *Proc. IEEE Int. Conf. Intell. Transp. Syst.*, Oct. 2014, pp. 334–341.

[39] Federal Highway Administration. (2006). *Next Generation Simulation (NGSIM) Program*. [Online]. Available: http://ngsim-community.org/

[40] M. Schreier, V. Willert, and J. Adamy, "An integrated approach to maneuver-based trajectory prediction and criticality assessment in arbitrary road environments," *IEEE Trans. Intell. Transp. Syst.*, vol. 17, no. 10, pp. 2751–2766, Oct. 2016.

[41] M. Baharam, C. Hubmann, A. Lawitzky, M. Aeberhard, and D. Wollherr, "A combined model- and learning-based framework for interaction-aware maneuver prediction," *IEEE Trans. Intell. Transp. Syst.*, vol. 17, no. 6, pp. 1538–1550, Jun. 2016.

[42] M. Baharam, A. Lawitzky, J. Friedrichs, M. Aeberhard, and D. Wollherr, "A game-theoretic approach to replanning-aware interactive scene prediction and planning," *IEEE Trans. Veh. Technol.*, vol. 65, no. 6, pp. 3981–3992, Jun. 2016.
[43] S. Noh and K. An, "Decision-making framework for automated driving in highway environments," *IEEE Trans. Intell. Transp. Syst.* [Online]. Available: http://ieeexplore.ieee.org/document/7907201/
[44] K. Jo, M. Lee, J. Kim, and M. Sunwoo, "Tracking and behavior reasoning of moving vehicles based on roadway geometry constraints," *IEEE Trans. Intell. Transp. Syst.*, vol. 18, no. 2, pp. 460–476, Feb. 2017.
[45] I. H. Kim, J.-H. Bong, J. Park, and S. Park, "Prediction of driver's intention of lane change by augmenting sensor information using machine learning techniques," *IEEE Sensors J.*, vol. 17, no. 6, p. 1350, Jun. 2017.

Jaehwan Kim (S'15) received the B.S. degree in mechanical engineering from Sogang University, Seoul, South Korea, in 2013 and the M.S degree from the Graduate School for Green Transportation, Korea Advanced Institute of Science and Technology, Daejeon, South Korea, in 2016.

He is currently with the Mando Global Research and Development Center, Gyeonggi-do, South Korea. His research of interests are risk assessment and collision avoidance in the autonomous driving vehicles.

Dongsuk Kum (M'13) received the Ph.D. degree in mechanical engineering from University of Michigan, Ann Arbor, MI, USA, in 2010. He is currently an Assistant Professor with the Graduate School for Green Transportation, Korea Advanced Institute of Science and Technology (KAIST) and the Director of the Vehicle Dynamics and Controls Laboratory. His research centers on the modeling, control, and design of advanced vehicular systems with particular interests in hybrid electric vehicles and autonomous vehicles.

Prior to joining KAIST, he was with the General Motors Research and Development Propulsion Systems Research Laboratory, Warren, MI, USA, as a visiting Research Scientist, where he was involved in advanced propulsion system technologies, including hybrid electric vehicles, flywheel hybrid, and waste heat recovery systems.